

Using wavelet analysis to compare the QCD prediction and experimental data on $R_{e^+e^-}$ and to determine parameters of the charmonium states above the $D\bar{D}$ threshold

V. K. Henner^{1,2,3,a}, C. L. Davis^{1,b}, T. S. Belozero²

¹ Department of Physics, University of Louisville, Louisville, KY 40292, USA

² Department of Theoretical Physics, Perm State University, Perm 614990, Russia

³ Department of Mathematics, Perm State Technical University, Perm 614990, Russia

Received: 19 June 2015 / Accepted: 21 October 2015 / Published online: 28 October 2015
© The Author(s) 2015. This article is published with open access at Springerlink.com

Abstract The first part of our analysis uses the wavelet method to compare the quantum chromodynamic (QCD) prediction for the ratio of hadronic to muon cross sections in electron-positron collisions, R , with experimental data for R over a center of mass energy range up to about 7 GeV. A direct comparison of the raw experimental data and the QCD prediction is difficult because the data have a wide range of structures and large statistical errors and the QCD description contains sharp quark-antiquark thresholds. However, a meaningful comparison can be made if a type of “smearing” procedure is used to smooth out rapid variations in both the theoretical and experimental values of R . A wavelet analysis (WA) can be used to achieve this smearing effect. The second part of the analysis concentrates on the 3.0–6.0 GeV energy region which includes the relatively wide charmonium resonances $\psi(1^-)$. We use the wavelet methodology to distinguish these resonances from experimental noise, background and from each other, allowing a reliable determination of the parameters of these states. Both analyses are examples of the usefulness of WA in extracting information in a model independent way from high energy physics data.

1 Wavelet transformations

Let us start with a brief description of the continuous wavelet transformation (WT). The WT of function $f(t)$ is defined by

$$w(a, t) = \frac{1}{\sqrt{aC_\varphi}} \int_{-\infty}^{+\infty} \varphi^* \left(\frac{t' - t}{a} \right) f(t') dt', \quad (1)$$

where C_φ is a normalization constant subject to the choice of wavelet. The decomposition described by Eq. (1) is performed by convolution of the function $f(t)$ with a bi-parametric family of self-similar functions generated by dilatation and translation of the analyzing function $\varphi(t)$ called a wavelet,

$$\varphi_{a,b}(t) = \varphi \left(\frac{t - b}{a} \right), \quad (2)$$

where the scale parameter a characterizes the dilatation, and b characterizes the translation. It is a kind of “window function” with a non-constant window width. High frequency wavelets are narrow due to the factor $1/a$, while low frequency wavelets are much broader. The function $\varphi(t)$ should be well localized in both time and Fourier space and must obey the admissibility condition, $\int_{-\infty}^{+\infty} \varphi(t) dt$. This condition requires $\varphi(t)$ must be an oscillatory function and, if the integral (1) converges, the completeness of the wavelet functions provides the existence of inverse transformation,

$$f(t) = \frac{1}{\sqrt{C_\varphi}} \int_{-\infty}^{+\infty} \int_0^{+\infty} \varphi \left(\frac{t - t'}{a} \right) w(a, t') \frac{dt' da}{a^{5/2}} dt. \quad (3)$$

In contrast to Fourier analysis, the WT depends both on t and the frequency providing an optimal compromise with the uncertainty principal. One of the advantages of wavelet analysis is a fairly low sensitivity of the restored signal to any physically reasonable continuation of the function $f(t)$ outside the interval (t_{min}, t_{max}) where the data are known. To fill in gaps between the experimental points we use a linear interpolation (different interpolations lead to minimal difference in the restored signal). Note that since the average value of any wavelet is zero, the mean value of the WT is zero, so that $\langle f \rangle$ must be added to the reconstructed signal to restore the mean value of the original signal.

^a e-mail: vkhen01@louisville.edu

^b e-mail: c.l.davis@louisville.edu

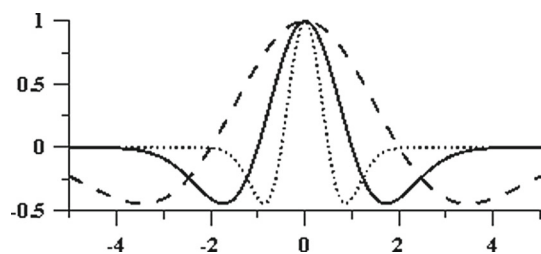


Fig. 1 Wavelet “Mexican Hat” $\varphi(t) = (1 - t^2)e^{-t^2/2}$. Solid line – $\varphi(t)$, dashed line – $\varphi(t/2)$, dotted line – $\varphi(t/0.5)$

Wavelets with good localization and a small number of oscillations are commonly used to recognize the local features of data, and to find the parameters of dominating structures (location and scale/width). In this work, we use one of the most popular wavelets of this type, the so-called “Mexican Hat”,

$$\varphi(t) = (1 - t^2)e^{-t^2/2}. \quad (4)$$

This wavelet is plotted in Fig. 1 for three values of the scale parameter, $a = 1, 2$ and 0.5 .

2 Wavelets and the R ratio

Our first goal is to use wavelet methodology to compare the QCD prediction of R to experimental data in the center of mass energy range up to about 7 GeV. In zeroth order in the strong coupling constant α_s , the ratio R is given by

$$R(Q) = \frac{\sigma(e^+e^- \rightarrow \text{hadrons})}{\sigma(e^+e^- \rightarrow \mu^+\mu^-)} \approx 3 \sum_q e_q^2 \equiv R^{(0)}(Q), \quad (5)$$

where the summation extends over the quark flavors $q = u, d, s, c$ available up to the center of mass energy Q . The QCD α_s corrections to $R^{(0)}(Q)$ can be presented in different forms. To be specific we adopt the form of reference [1],

$$R(Q) = 3 \sum_q e_q^2 T(v_q) [1 + g(v_q) \mathcal{R}], \quad (6)$$

where

$$\begin{aligned} \mathcal{R} &= \frac{\alpha_s}{\pi} \left[1 + \frac{\alpha_s}{\pi} + C_2 \left(\frac{\alpha_s}{\pi} \right)^2 + C_3 \left(\frac{\alpha_s}{\pi} \right)^3 + \dots \right], \\ v_q &= \left[1 - 4m_q^2/Q^2 \right]^{1/2}, \quad T(v) = v(3 - v^2)/2, \\ g(v) &= \frac{4\pi}{3} \left[\frac{\pi}{2v} - \frac{3+v}{4} \left(\frac{\pi}{2} - \frac{3}{4\pi} \right) \right] \end{aligned}$$

and the summation in (6) is over all quark flavors whose masses m_q are less than $Q/2$. For this analysis we use the

quark masses, the form of the coefficients C_2 and C_3 calculated in [3,4] and the energy dependence of $\alpha_s(Q^2)$ from [2].

It is very hard to determine the role of these QCD corrections by comparison with experimental data for $R(Q)$ due to the large statistical errors and plethora of overlapping and interfering resonances in this region. An additional complicating factor is that the QCD perturbative approach exhibits sharp quark-antiquark thresholds. However, a meaningful comparison can be made by applying some type of “smearing” procedure, which has the effect of smoothing out rapid variations in both the theoretical and experimental values of R .

Before describing our wavelet analysis of this data it is worth considering the methodology developed in references [1,2] to compare experimental data and QCD predictions. The smearing procedure used in these analyses calculates a smeared ratio R as follows,

$$R(s, \Delta) = \frac{\Delta}{\pi} \int_0^{s_{\max}} \frac{R(s')}{(s' - s)^2 + \Delta^2} ds', \quad (7)$$

where $\sqrt{s} = Q$ is the square of the center of mass energy and Δ is the “smearing” parameter. In references [1,2] to evaluate the integral (7), it was necessary to exclude sharp resonances, such as the $\psi(3.100)$ and the much wider ρ peak. In addition, a term is added to account for the contribution from s_{\max} to ∞ , assuming that R remains constant above $s_{\max} \approx 60 \text{ GeV}^2$. Originally, the smearing procedure in reference [1] supposes a global constant value $\Delta = 3 \text{ GeV}^2$ in (7). However it was found in reference [2] that for different energy regions it would be better to use different values of Δ . Note that the use of an energy dependent Δ in (7) reflects the necessity for different treatment of different energy scales.

The WT methodology provides an alternative, model independent, smearing method, which does not require different treatment in differing energy scales. Under WT to separate the signal from the background noise, wavelet reconstruction is performed for scales greater than a certain scale a_{noise} —the boundary, or cut-off, scale [5]. In deciding on the appropriate boundary scale that will separate the noise-like high frequency components of the data we take a pragmatic line of reasoning. That is, the best choice for a_{noise} is the smallest value which will smooth out any rapid variations in the data enabling us to reproduce stable results for low frequencies (resonance area). A similar pragmatic strategy was applied in the analyses of [1,2] in choosing the parameter Δ of equation (7). The best value of Δ is large enough to compare the smeared R with QCD models, but not so large that all the fine detail of the data is smoothed away.

Figure 2 displays wavelet reconstructed (smeared) experimental data with cut-off values $a_{\text{noise}} = 0.6$ (bold dashed curve) and $a_{\text{noise}} = 1.2$ (bold solid curve). The data is a com-

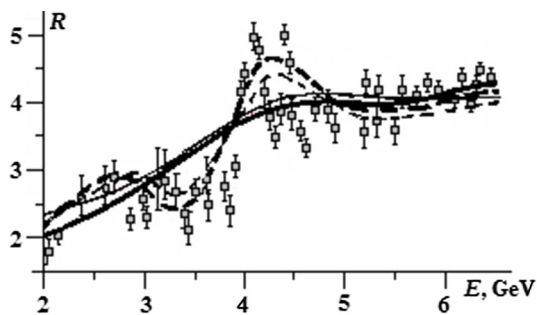


Fig. 2 Wavelet reconstruction of $R_{e^+e^-}$. Dashed and solid bold curves correspond to wavelet reconstruction of the experimental data with $a_{noise} = 0.6$ and $a_{noise} = 1.2$, respectively. Dashed and solid thin curves correspond to wavelet reconstruction of QCD calculations (6) with the same a_{noise} values

pilation of measurements from many different experiments obtained from the Particle Data Group (PDG) [6]. In contrast to the analyses of [1, 2], under the WT approach there is no need to remove sharp resonances ($\psi(3.100)$ etc.) by hand, they effectively become part of the high frequency noise and the wavelet analysis smears them out. The thin dashed line and thin solid line are wavelet reconstructed QCD curves with $a_{noise} = 0.6$ and $a_{noise} = 1.2$, respectively. As can be seen, the two curves with $a_{noise} = 1.2$, representing experiment and theory, are in good agreement. It should be noted that the contribution to all of the restored data curves in Fig. 2 from the data region above 6.5 GeV is negligible.

3 ψ states above the $D\bar{D}$ threshold and the wavelet procedure

Detailed information on the charmonium resonances $\psi(1^-)$ above the $D\bar{D}$ threshold at 3.73 GeV comes primarily from the measurement of $R_{e^+e^-}$. This data, provided by the Particle Physics Data Group (PDG) [6], comes from the work of many experimental collaborations over a period of more than 30 years. Several broad vector resonances are observed with varying degrees of clarity. The current best estimate of the masses and widths from the PDG are presented in Table 1.

The main difficulty encountered by each of the collaborations in making these measurements is large statistical errors and hence the difficulty of separating resonance “sig-

nal” from noise. There is significant disagreement between the collaborations on many of the resonance parameters. Therefore, due to the possibility of systematic errors we do not combine measurements from different experiments, but choose to base this initial analysis on data from the BES collaboration which exhibits clear evidence of four broad resonances above the $D\bar{D}$ threshold. In addition to the PDG values, Table 1 shows the masses and widths of these resonances from the most recent BES analysis [7].

Before analyzing the charmonium resonances parameters, we first determine the non-resonant background contribution using a WT followed by wavelet reconstruction. This methodology, with its excellent scaling property, allowing the analysis of data with varying resolution, is ideally suited to separate resonances from noise, background and each other. A very helpful representation of the WT revealing all the features of the complete spectrum of the signal is the “time-frequency” plane (Fig. 3a). This is a multi-resolution spectrogram, which shows the frequency (scale) contents of the signal as a function of energy. Each pixel on the spectrogram represents $w(a, t)$ for a particular a (scale) and t (in our case t is energy, $E \equiv Q$). The location of spots on the vertical axis (scale axis, a) corresponds to the width of the maximum. The intensity of dark spots shows the amplitudes of maxima. The WT image (wavelet plane) of the BES charmonium data obtained with the “Mexican Hat” wavelet is shown in panel (a) of Fig. 3. The WT localizes the structures in a fashion that allows us to estimate the masses of the resonances and their widths—all four ψ resonances are clearly seen on the wavelet plane. The straight horizontal line corresponds to the boundary scale a_{noise} , which can be chosen to cut off small scale structures, which in this case corresponds to experimental noise. By choosing a larger value of a_{noise} it is possible to also cut out the resonances, leaving only the background. The background curves for three substantially different choices of a_{noise} (0.15, 0.25 and 0.35) are displayed in Fig. 3b). In the following analysis we show that the charmonium resonance parameters are not sensitive to the choice of a_{noise} .

For each value of a_{noise} we subtract this “wavelet background” from the raw experimental data leaving only the contribution from the broad charmonium resonances. We then perform a least squares fit of the “signal” in this energy range to the sum of four Breit-Wigner resonances of the form,

Table 1 Properties of vector (charmonium) resonances above the charm threshold from the PDG and the BES [7] collaboration

Resonance	Mass (GeV)		Full Width (GeV)	
	PDG [6]	BES [7]	PDG [6]	BES [7]
$\psi(3.770)$	3.773 ± 0.0003	3.772 ± 0.002	0.027 ± 0.001	0.030 ± 0.009
$\psi(4.040)$	4.039 ± 0.001	4.040 ± 0.004	0.080 ± 0.010	0.085 ± 0.012
$\psi(4.160)$	4.191 ± 0.005	4.192 ± 0.007	0.103 ± 0.008	0.072 ± 0.012
$\psi(4.415)$	4.421 ± 0.004	4.415 ± 0.008	0.062 ± 0.020	0.072 ± 0.019

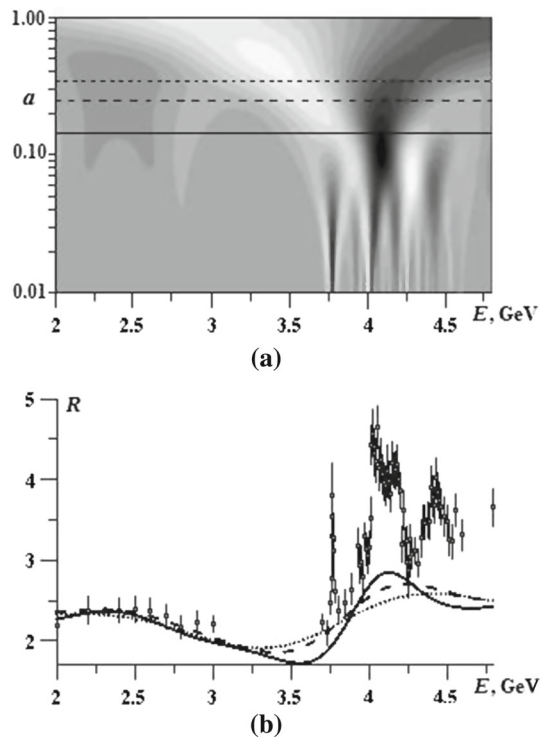


Fig. 3 **a** Wavelet plane for $a \in [0.01, 1]$; **b** background for $a_{noise} = 0.15$ (solid line), $a_{noise} = 0.25$ (dashed line), $a_{noise} = 0.35$ (dotted line)

$$R_{res} = \frac{9}{\alpha_{em}^2} \sum_{r=1}^4 B_{lr} B_{hr} \frac{M_r^2 \Gamma_r^2}{(s - M_r^2)^2 + M_r^2 \Gamma_r^2}, \quad (8)$$

where M_r , Γ_r , B_{lr} and B_{hr} are, respectively, the mass, total width, leptonic branching fraction and hadronic branching fraction of the resonance. Each Breit-Wigner has three fitted parameters, M , Γ and the product of B_{lr} and B_{hr} . It is worth noting that since these resonances partially overlap, if their

Table 2 Breit-Wigner fitted parameters for $a_{noise} = 0.15$

Resonance	Mass (GeV)	Width (GeV)	$B_l B_h \cdot 10^5$
$\psi(3.770)$	3.772 ± 0.0002	0.032 ± 0.005	0.983 ± 0.076
$\psi(4.040)$	4.042 ± 0.001	0.088 ± 0.013	0.921 ± 0.067
$\psi(4.160)$	4.161 ± 0.006	0.100 ± 0.019	0.664 ± 0.069
$\psi(4.415)$	4.430 ± 0.007	0.098 ± 0.014	0.936 ± 0.071

Table 3 Breit-Wigner fitted parameters for $a_{noise} = 0.25$

Resonance	Mass (GeV)	Width (GeV)	$B_l B_h \cdot 10^5$
$\psi(3.770)$	3.772 ± 0.0001	0.022 ± 0.004	0.888 ± 0.094
$\psi(4.040)$	4.043 ± 0.003	0.097 ± 0.011	1.110 ± 0.064
$\psi(4.160)$	4.185 ± 0.005	0.083 ± 0.016	0.715 ± 0.077
$\psi(4.415)$	4.423 ± 0.004	0.090 ± 0.016	0.819 ± 0.076

Table 4 Breit-Wigner fitted parameters for $a_{noise} = 0.35$

Resonance	Mass (GeV)	Width (GeV)	$B_l B_h \cdot 10^5$
$\psi(3.770)$	3.773 ± 0.0001	0.022 ± 0.004	0.888 ± 0.090
$\psi(4.040)$	4.043 ± 0.003	0.097 ± 0.011	1.155 ± 0.061
$\psi(4.160)$	4.165 ± 0.004	0.083 ± 0.013	0.907 ± 0.073
$\psi(4.415)$	4.423 ± 0.004	0.090 ± 0.014	0.889 ± 0.071

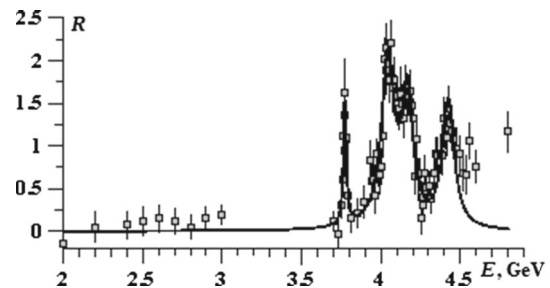


Fig. 4 Breit-Wigner fit of BES data with “wavelet background” subtracted, $a_{noise} = 0.35$

decay channels are specified, we can improve their resolution by using the multi-channel unitary scheme described in reference [8]. We defer this investigation to a future analysis.

The values of the fitted parameters for each of the four Breit-Wigner resonances for backgrounds obtained with three different values of a_{noise} are presented in Tables 2, 3 and 4. The chi squared per degree of freedom for the three fits are 1.11, 1.22 and 0.99 for the a_{noise} values of 0.15, 0.25 and 0.35, respectively.

As can be seen in Tables 2, 3, and 4, the fitted parameters of the four charmonium resonances are not significantly different for the three values of a_{noise} . Therefore, in Fig. 4 we present only the fitted curve (8) for $a_{noise} = 0.35$.

It should be noted that in this analysis, after subtracting the wavelet background, we exclude the four highest energy data points from the fitting procedure. Without these points the $\psi(4.415)$ resonance is “well-shaped”; if these four points are included the resonance is no longer “well-shaped” and its width is about twice that of the values presented in Table 1.

Justification for excluding the four highest energy points can be made as follows. If instead of the wavelet fitted background we fit the data with four Breit-Wigners and a parabolic (or linear) background, including the four highest energy data points, we see that the fourth resonance is not “well-shaped” and the last few data points appear to be associated with the background rather than the 4th resonance, see Fig. 5. Furthermore, the fitted width of this fourth resonance (Table 5) is significantly larger than that of the second and third resonances and the published PDG value. In order to show the association of the highest energy points with the parabolic background we do not subtract the background in Fig. 5. It should be emphasized that inclusion or exclusion of these

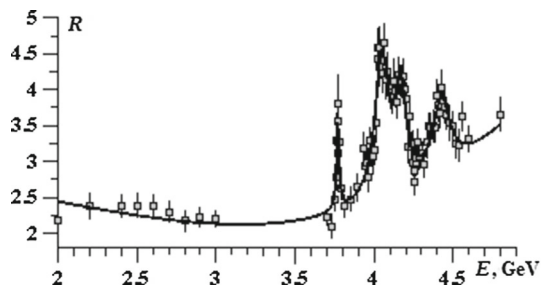


Fig. 5 Breit-Wigner and parabolic background fit of BES data (contrary to Fig. 4 the background is not subtracted from the data)

Table 5 Breit-Wigner parameters for fit with parabolic background

Resonance	Mass (GeV)	Width (GeV)	$B_l B_h \cdot 10^5$
$\psi(3.770)$	3.770 ± 0.001	0.021 ± 0.004	1.202 ± 0.097
$\psi(4.040)$	4.048 ± 0.003	0.107 ± 0.010	1.946 ± 0.079
$\psi(4.160)$	4.166 ± 0.003	0.086 ± 0.013	1.335 ± 0.067
$\psi(4.415)$	4.426 ± 0.005	0.148 ± 0.022	1.001 ± 0.085

four data points does not significantly alter the background curve obtained via the wavelet method and that the choice of a polynomial background is arbitrary, whereas the wavelet background is obtained from the data itself in a model independent manner.

To demonstrate the reliability of our WT methodology in extracting the parameters of these charmonium resonances we performed a study using simulated data as follows. Starting from the PDG values of masses and widths of the four charmonium resonances given in Table 1 we generate a spectrum of four Breit-Wigners of the basic form of Eq. (8). To simulate real experimental data we discretize the spectrum from 2.0 to 5.5 GeV in 0.05 GeV intervals, then add a random vertical shift from -0.2 to $+0.2$ and random error bars in the range 0.15 – 0.4 to the data points. To complete the simulated data spectrum a representative background curve is added to the data points. Finally we pass this simulated data through the same WT analysis chain applied to the real data. This gives us a wavelet background curve and the masses and widths of the Breit-Wigner resonances after the wavelet background subtracted fit. In addition to applying our WT methodology to the simulated data we perform a Breit-Wigner and parabolic background fit in exactly the same way as we did for the real data.

This study was performed for several different initial background curves. In all such cases the WT methodology accurately reproduced the input background shape. Fitting the wavelet background subtracted simulated data, as described above, also accurately reproduces the masses and widths of the assigned Breit-Wigner resonances, independent of the particular input background curve. The parabolic background least squares fit of the simulated data was also able to

reproduce the Breit-Wigner masses and widths, but in contrast led to fitted backgrounds very different from the input background. We believe the fact that the masses and widths were accurately reproduced, despite the fitted background being very different from the input background, is largely due to the clean nature of the simulated data. Real experimental data is clearly more complex, in which case the inability of the standard parabolic background least squares fit to extract an accurate background could lead to less reliable resonance parameters.

4 Conclusion

Experimental measurements of the ratio, R , comprise a wide range of structures with large statistical errors, making direct comparison with the predictions of QCD very difficult. However, a meaningful comparison can be made provided that some kind of “smearing” procedure, similar to that described in [1], is used to smooth out rapid variations in R . A wavelet analysis can be used to achieve this smearing effect. We compare the WT of the predictions of perturbative QCD and experimental R data. The wavelet reconstruction of the R experimental data preserves its main features, but with damped statistical errors and threshold singularities. The WT of QCD perturbation theory is in good general agreement with the WT experimental data.

Using the wavelet methodology to obtain the background in the charmonium energy range above the naked charm threshold provides an important, model independent, alternative to other accepted methods. The masses and widths of the four vector mesons above the charm threshold, $\psi(3.700)$, $\psi(4.040)$, $\psi(4.160)$ and $\psi(4.415)$, obtained from fitting wavelet background subtracted data from the BES experiment, are found to be largely insensitive to the specific choice of the WT parameters and consistent with the BES and PDG reported values.

Acknowledgments The authors wish to thank Harrison Simrall and Adam Redwine for their work on the fitting algorithm and A. L. Kataev for useful advice.

Open Access This article is distributed under the terms of the Creative Commons Attribution 4.0 International License (<http://creativecommons.org/licenses/by/4.0/>), which permits unrestricted use, distribution, and reproduction in any medium, provided you give appropriate credit to the original author(s) and the source, provide a link to the Creative Commons license, and indicate if changes were made. Funded by SCOAP³.

References

1. E.C. Poggio, H.R. Quinn, S. Weinberg, Phys. Rev. D **13**, 1958 (1976)
2. A.C. Mattingly, P.M. Stevenson, Phys. Rev. D **49**, 437 (1994)

3. S.G. Gorishney, A.L. Kataev, S.A. Larin, Phys. Lett. B **259**, 144 (1991)
4. L.R. Surguladze, M.A. Samuel, Phys. Rev. Lett. **66**, 560 (1991). [Erratum *ibid* **66**, 2416 (1991)]
5. V.K. Henner, P.G. Frick, T.S. Belozeroва, V.G. Solov'yev, Eur. Phys. J. C **26**, 3 (2002)
6. Review of Particle Physics by the Particle Physics Data Group, Chin. Phys. C **38**, 090001 (2014)
7. M. Ablikim et al. [BES Collaboration], Phys. Lett. B **660**, 315 (2008)
8. T.S. Belozeroва, V.K. Henner, Phys. Part. Nuclei **29**, 63 (1998)